Gyrokinetic particle simulation of fast-electron driven beta-induced Aflvén eigenmode

Junyi Cheng,[1,2] Wenlu Zhang,[2,1,3,a)] Zhihong Lin,[3,4] Ihor Holod,[3] Ding Li,[2,1] Yang Chen,[1,2] and Jintao Cao[2]
[1]*Department of Modern Physics, University of Science and Technology of China, Hefei, Anhui 230026, China*
[2]*Beijing National Laboratory for Condensed Matter Physics and CAS Key Laboratory of Soft Matter Physics, Institute of Physics, Chinese Academy of Sciences, Beijing 100190, China*
[3]*Department of Physics and Astronomy, University of California, Irvine, California 92697, USA*
[4]*Fusion Simulation Center, Peking University, Beijing 100871, China*

(Received 1 March 2016; accepted 15 April 2016; published online 5 May 2016)

The fast-electron driven beta-induced Alfvén eigenmode (e-BAE) in toroidal plasmas is investigated for the first time using global gyrokinetic particle simulations, where the fast electron is described by the drift kinetic equation. The simulation shows that the e-BAE propagates in the fast electron diamagnetic direction and its polarization is close to an ideal MHD mode. The phase space structure shows that only the fast electron processional resonance is responsible for the e-BAE excitations while fast-ion driven BAE can be excited through all the channels, including transit, bounce, and processional resonance. *Published by AIP Publishing.*
[http://dx.doi.org/10.1063/1.4948487]

I. INTRODUCTION

The Alfvén waves, which were predicted by Alfvén in 1942,[1] are low frequency waves commonly observed in the space and laboratory plasma environment. In the magnetic confinement fusion plasma, energetic particles, including fast ions and fast electrons produced by the fusion reaction and auxiliary heating, can excite various Alfvén instabilities, which may induce significant transport[2–4] and degrade the overall plasma confinement. The β-induced Alfvén eigenmode (BAE) is formed by the finite compressibility induced by the geodesic curvature of the equilibrium magnetic field and the plasma pressure.[5–7] Its frequency falls in the so-called β-induced Alfvén frequency gap,[5,8] where the normalized pressure β is the ratio between plasma pressure and magnetic pressure. The frequency of BAE is of the order of thermal ion transit frequency,[6] which makes the BAE subject to the strong interaction with the thermal ions.[9] The weakly damped BAE excited by pressure gradients of fast ions or fast electrons was first observed with the beam ion in DIII-D[10] and TFTR.[11,12] Subsequently, BAE were also observed during the tearing mode activities in FTU,[13,14] TEXTOR,[15] and HL-2A.[16] Additionally, BAE was observed during the ion cyclotron heating in Tore-Supra.[17] The Alfvén instabilities related to fast electrons were observed, such as internal kink mode and fishbone in DIII-D[18] and BAE and fishbone in HL-2A.[19,20] The fast-electron driven β-induced Alfvén eigenmode (e-BAE) was identified for the first time both in the Ohmic and electron cyclotron resonance heating (ECRH) plasma in HL-2A.[20,21] Meanwhile, the BAE excitation has different explanations by several theories, such as the discrete shear Alfvén eigenmode (AE),[8] the kinetic ballooning mode (KBM),[22] the energetic particle mode,[23–25] the hybrid mode between Alfvénic and KBM branches, or between Alfvénic and ion acoustic branches.[26]

The BAE driven by the fast ion (i-BAE) has been extensively investigated through experimental, simulation, and theoretical studies. By contrast, e-BAE has been much less explored. In this paper, an electromagnetic gyrokinetic toroidal code (GTC)[27,28] is used to simulate the e-BAE, where fast electrons are described by the drift kinetic model. GTC has been successfully applied to the simulation of microturbulence,[29–31] pressure-driven Alfvén eigenmodes (AEs),[32–37,42–45] current-driven instabilities,[46,47] and radio frequency waves[48,49] in fusion plasmas. GTC simulation of antenna-excited BAE, linear,[43] and nonlinear i-BAE[44,45] has been carried out by Zhang. Meanwhile, by using an MHD-gyrokinetic hybrid code XHMGC,[50,51] the simulation of the discrete kinetic BAE (KBAE)[52] and nonlinear i-BAE[53] has been performed by Wang. A particle/MHD hybrid code, M3D,[54] has been used to simulate BAEs with NSTX parameters[55] and found that the BAE is sensitive to the thermal ion's β.

In this work, the BAE is successfully excited by the fast electron density gradient in GTC linear simulations. The simulations show that e-BAE propagates in the fast electron diamagnetic direction, as observed in the experiment in HL-2A.[20] The simulations show that the polarization of e-BAE is closed to an ideal MHD mode. Its frequency changes slightly as the fast electron temperature, density, or density gradient changes. The growth rate increases slightly when the amplitude of the fast electron temperature, density, or density gradient increases. And the thermal plasma properties, such as aspect ratio and pressure, will influence the e-BAE frequency and linear growth rate. According to the phase space structure for the fast electron perturbed distribution function, only the processional resonance is responsible for the e-BAE excitation.

a)Electronic mail: wzhang@iphy.ac.cn

This paper is organized as follows: physical model for e-BAE simulation in GTC is presented in Sec. II. In Sec. III, the gyrokinetic simulation results of e-BAE excited by fast electrons are presented. Section IV is the summary.

II. PHYSICAL MODEL FOR e-BAE SIMULATION

The gyrokinetic equations[56] are used to describe the plasma of toroidal systems in five-dimensional phase space

$$\frac{d}{dt}f_\alpha(\mathbf{X},\mu,v_\parallel,t)\equiv\left[\frac{\partial}{\partial t}+\dot{\mathbf{X}}\cdot\nabla+\dot{v}_\parallel\frac{\partial}{\partial v_\parallel}-\mathcal{C}_\alpha\right]f_\alpha=0, \quad (1)$$

$$\dot{\mathbf{X}}=v_\parallel\frac{\mathbf{B}}{B_0}+\mathbf{v}_E+\mathbf{v}_c+\mathbf{v}_g, \quad (2)$$

$$\dot{v}_\parallel=-\frac{1}{m_\alpha}\frac{\mathbf{B}^*}{B_0}\cdot(\mu\nabla B_0+Z_\alpha\nabla\phi)-\frac{Z_\alpha}{m_\alpha c}\frac{\partial A_\parallel}{\partial t}, \quad (3)$$

where gyro-center position $\mathbf{X}$, magnetic moment μ, and parallel velocity $v_\parallel$ are selected as a set of complete independent variables, and the index $\alpha=i,e,fe$ stands for the particle species of thermal ion, thermal electron, and fast electron, respectively. Z_α is the particle charge, m_α is the particle mass, and ϕ and $A_\parallel$ are the electrostatic potential and the vector potential parallel to $\mathbf{B}_0$, respectively. Here, $\mathbf{B}_0\equiv B_0\mathbf{b}_0$ is the equilibrium magnetic field, $\mathbf{B}=\mathbf{B}_0+\delta\mathbf{B}$, $\mathbf{B}^*=\mathbf{B}_0^*+\delta\mathbf{B}$, $\mathbf{B}_0^*=\mathbf{B}_0+(B_0v_\parallel/\Omega_\alpha)\nabla\times\mathbf{b}_0$, Ω_α is the cyclotron frequency of species α. In the lowest order, the perturbed magnetic field is prescribed as $\delta\mathbf{B}=\nabla\times(A_\parallel\mathbf{b}_0)$, so the compressional component of the magnetic field perturbation is excluded by assuming $\delta B_\parallel=0$. The $\mathbf{E}\times\mathbf{B}$ drift $\mathbf{v}_E$, magnetic curvature drift $\mathbf{v}_c$, and grad-$\mathbf{B}$ drift $\mathbf{v}_g$ are given by

$$\mathbf{v}_E=\frac{c\mathbf{b}_0\times\phi}{B_0}, \quad (4)$$

$$\mathbf{v}_c=\frac{v_\parallel^2}{\Omega_\alpha}\nabla\times\mathbf{b}_0, \quad (5)$$

$$\mathbf{v}_g=-\frac{\mu}{m_\alpha\Omega_\alpha}\mathbf{b}_0\times\nabla B_0. \quad (6)$$

Since the Larmor radius of the fast electron is much smaller than the spatial characteristic scale of BAE which is of the same order of the thermal ion Larmor radius, the drift-kinetic limit is taken for the fast electron while the thermal ion is simulated with the finite Larmor effect. The fast electrons have much higher velocity than the thermal ions, so in the simulation, a technique of the time step, namely the sub-cycling method, is used to save the computing time while maintaining the precision. Specifically, the method is to push electrons several times for each time step of pushing ions and field updates. Meanwhile, a larger particle number of fast electrons in PIC simulation is needed to reduce the velocity space numeric noise.

When the Aflvén instabilities are driven by fast electrons, the fast electron processional resonance has a significant effect and the non-adiabatic response of the fast electron can not be treated as a high-order term compared with the adiabatic response, so the fast electron is described in the drift kinetic model. On the other hand, for the fast-electron driven Alfvén instabilities, the kinetic effect of the thermal electron is much smaller. Thus the thermal electron description can be further simplified to the fluid-kinetic hybrid electron model,[28,36,58–60] which consists of a lowest-order adiabatic part and a high-order non-adiabatic part with linear and nonlinear kinetic terms. This model has better efficiency and numerical properties for low frequency ($\omega\ll k_\parallel v_\parallel$) modes.

In the lowest order of the fluid-kinetic hybrid model, the adiabatic response of thermal electrons can be described by the fluid continuity equation by integrating Eq. (1) in the velocity space in the drift-kinetic limit and keeping the first-order terms

$$\frac{\partial\delta n_e}{\partial t}+B_0\mathbf{b}_0\cdot\nabla\left(\frac{n_{0e}\delta u_{\parallel e}}{B_0}\right)+B_0\mathbf{v}_E\cdot\nabla\left(\frac{n_{0e}}{B_0}\right)-n_{0e}(\mathbf{v}_*+\mathbf{v}_E)\cdot\frac{\nabla B_0}{B_0}=0, \quad (7)$$

where $\mathbf{v}_*=\mathbf{b}_0\times\nabla(\delta P_{e\parallel}+\delta P_{e\perp})/(n_{0e}m_e\Omega_e)$, $\delta P_{e\parallel}=\int d\mathbf{v}\, mv_\parallel^2\delta f_e$, $\delta P_{e\perp}=\int d\mathbf{v}\mu B_0\delta f_e$. $\delta n_e=\int d\mathbf{v}\delta f_e$ is the perturbed thermal electron density, $n_{0e}\delta u_{e\parallel}=\int d\mathbf{v}v_\parallel\delta f_e$ is the perturbed thermal electron current, $n_{0e}=\int d\mathbf{v}f_{0e}$, f_{0e} is the equilibrium distribution function of the thermal electron, $\delta f_e=f_e-f_{0e}$ is the perturbed distribution function of the thermal electron. Note that $\int d\mathbf{v}=\int_0^{+\infty}d\mu\int_{-\infty}^{+\infty}dv_\parallel 2\pi B_0/m$.

The parallel fluid velocity of the thermal electron in the above equation can be calculated by using the parallel Ampère's law

$$en_{0e}\delta u_{\parallel e}=\frac{c}{4\pi}\nabla_\perp^2A_\parallel+Z_in_{0i}\delta u_{\parallel i}-en_{0fe}\delta u_{\parallel fe}. \quad (8)$$

Meanwhile, the vector potential $A_\parallel$ is obtained by using the Faraday's law

$$\frac{1}{c}\frac{\partial A_\parallel}{\partial t}=-\mathbf{b}_0\cdot\nabla\phi-\delta E_\parallel=\mathbf{b}_0\cdot\nabla(\phi_{eff}-\phi). \quad (9)$$

The effective potential ϕ_{eff} is calculated by integrating the leading order terms of $\omega/(k_\parallel v_\parallel)$ in the electron gyrokinetic equation

$$\frac{e\phi_{eff}}{T_e}=\frac{\delta n_e}{n_{0e}}-\frac{\delta\psi}{n_{0e}}\frac{\partial n_{0e}}{\partial\psi_0}, \quad (10)$$

where ψ_0 and $\delta\psi$ are the equilibrium and perturbed poloidal flux, respectively. And $\partial\delta\psi/\partial t=-c\partial(\phi_{eff}-\phi)/\partial\alpha_0$, where $\alpha_0=q(\psi_0)\theta-\zeta$ is the magnetic field line label in terms of the poloidal angle θ and toroidal angle ζ in the magnetic coordinate.

In the lowest order, the pressure term in Eq. (7) can be written

$$\delta P_{e\parallel}=\delta P_{e\perp}=en_{0e}\phi_{eff}+\frac{\partial n_{0e}T_e}{\partial\psi_0}\delta\psi. \quad (11)$$

The system is closed with the gyro-kinetic Poisson's equation[61]

$$\frac{Z_i^2n_i}{T_i}(\phi-\tilde{\phi})=\sum_{\alpha=e,i,fe}Z_\alpha\delta n_\alpha, \quad (12)$$

where $\tilde{\phi} = \sum_k \phi_k \Gamma_0(k_\perp^2 \rho_i^2)$ is the second gyro-phase-averaged electrostatic potential.[62]

Next, we show that the gyro-kinetic simulation model can recover the ideal MHD results.[43] We reduce our equations in the limit of long wavelength, no parallel electric field $\delta E_\parallel = 0$, and $\nabla \times \mathbf{B}_0 \approx 0$. Eq. (12) becomes

$$\nabla_\perp \cdot \left(\frac{\nabla_\perp \phi}{v_A^2}\right) = -\frac{4\pi}{c^2} \sum_{\alpha=e,i,fe} Z_\alpha \delta n_\alpha, \tag{13}$$

where $v_A = B/\sqrt{4\pi n_i m_i}$ is the Alfvén velocity. By using Eq. (7) for all species, Eq. (8) and charge neutrality $\sum_\alpha Z_\alpha n_{0\alpha} = 0$, we can get

$$\frac{\partial^2}{\partial t^2}\left[\nabla_\perp \cdot \left(\frac{\nabla_\perp \phi}{v_A^2}\right)\right] - \frac{\partial}{\partial t}\frac{4\pi}{c}\nabla \cdot \left(\frac{\mathbf{b}_0}{B_0} \times \nabla \delta P\right) - \mathbf{B}_0 \cdot \nabla\left[\frac{1}{B_0}\nabla^2(\mathbf{b}_0 \cdot \nabla\phi)\right] = 0, \tag{14}$$

with $\delta P = \delta P_e + \delta P_i + \delta P_{fe}$, assuming that all species are isotropic. Eq. (14) is well known as the vorticity equation,[22,63] simplified with the above assumptions that neglect pressure gradient of thermal plasmas, finite Larmor radius effect, kinetic effect and equilibrium current drive. The terms in Eq. (14) are the inertial term, interchange term and field line bending term, respectively. The Alfvén accumulation point frequency of BAE can be obtained from the balance of the inertial and interchange terms.

Next, we derive the BAE linear relation by only considering the fluid electron pressure for simplicity. In toroidal geometry, the perturbed quantities with frequency ω and mode number (n, m) can be expressed as

$$\phi(r, \theta, \zeta, t) = \hat{\phi}(r) \exp[i(n\zeta - m\theta - \omega t)]. \tag{15}$$

The perturbed diamagnetic flow [the fourth term in Eq. (7)] can be neglected since it is smaller in comparison with the $E \times B$ convection [third term in Eq. (7)] by the factor $L_n/R_0 \ll 1$, where L_n is the thermal ion density gradient. Meanwhile, the $k_\parallel$ term is negligible in Eq. (7) since $k_\parallel \approx 0$ around the resonance surface for BAE. Then Eq. (7) is reduced to

$$\frac{\partial \delta n_e}{\partial t} = -n_{0e}\nabla \cdot \frac{c\nabla\phi \times \mathbf{B}_0}{B_0^2}. \tag{16}$$

For the uniform thermal electron, n_{0e} and T_e are independent of the ψ_0, so we can get $\delta P_e = \delta n_e T_e = e n_{0e} \phi_{eff}$. By using $\delta P_e = \delta \delta n_e T_e$ and Eq. (16), the second term in Eq. (14) becomes

$$-\frac{\partial}{\partial t}\frac{4\pi}{c}\nabla \cdot \left(\frac{\mathbf{b}_0}{B_0} \times \nabla \delta P_e\right) = n_{0e} T_e \nabla\left(\nabla\phi \cdot \nabla \times \frac{\mathbf{B}_0}{B_0^2}\right) \cdot \nabla \times \frac{\mathbf{B}_0}{B_0^2}. \tag{17}$$

Ignoring the $O(\epsilon^2/q^2)$ term and performing flux average, Eq. (14) becomes[43]

$$\frac{1}{r}\frac{d}{dr} r\left(\frac{\omega^2}{v_A^2} - k_\parallel^2 - \frac{2C_s^2}{v_A^2 R_0^2}\right)\frac{d}{dr}\hat{\phi} - \frac{m^2}{r^2}\left(\frac{\omega^2}{v_A^2} - k_\parallel^2 - \frac{2C_s^2}{v_A^2 R_0^2}\right)\hat{\phi} - \frac{k_\parallel}{r}\frac{d(k'_\parallel r)}{dr}\hat{\phi} = 0. \tag{18}$$

Here, $C_s^2 = T_e/m_i$ and $k_\parallel = (n - m/q)/R_0$, where m_i is the ion mass. When $k_\parallel = 0$, the accumulation point frequency is $\omega^2 = 2C_s^2/R_0^2$. More generally, the accumulation point frequency[6] including the pressure of the thermal plasma is

$$\omega_{\mathrm{BAE}} = \sqrt{\left(\frac{7}{2}T_i + 2T_e\right)/(m_i R_0^2)}. \tag{19}$$

III. GTC SIMULATION RESULTS OF e-BAE

In this work, an equilibrium with a concentric cross-section has been used for simplicity. The safety factor profile is $q = 1797 + 08(\psi/\psi_w) - 02(\psi/\psi_w)^2$, where ψ is the poloidal flux, ranging from $\psi = 0$ on axis to $\psi = \psi_w$ at the plasma boundary. The inverse aspect ratio is $\epsilon \equiv a/R_0 = 0.333$ in terms of tokamak minor radius a at wall and on-axis major radius R_0. The $q = 2$ rational surface is located at minor radius $r = 0.5a$ (r is the local minor radius). The thermal electron density n_{0e} is uniform and the fast electron density profile is $n_{fe} = 005 n_0(10 + 020(\tanh((026 - \psi/\psi_w)/006) - 10))$, so the fast electron density gradient reaches its maximum with $R_0/L_n = 17.2$ near q = 2 surface, where L_n is the density gradient scale length of fast electron. The thermal ion density n_{0i} is obtained by the quasi-neutral condition $Z_i n_{0i} = n_{0e} + n_{fe}$, where the thermal ion's charge number $Z_i = 1$. The thermal plasma temperature is uniform with $T_i = T_e$. The fast electrons are loaded as a local Maxwellian distribution for simplicity with uniform temperature $T_{fe} = 25T_e$. The thermal plasmas on-axis beta is $\beta = 4\pi n_0(T_e + T_i)/B_0^2 = 0.00718$ with B_0 being the on-axis magnetic field. The simulations are linear, and a toroidal mode filter is used to select only the toroidally most unstable mode $n = 3$, which has $k_\theta \rho_i = 0.047$ at the $q = 2$ rational surface with $a = 179\rho_i$. $k_\theta = nq/r$ is the

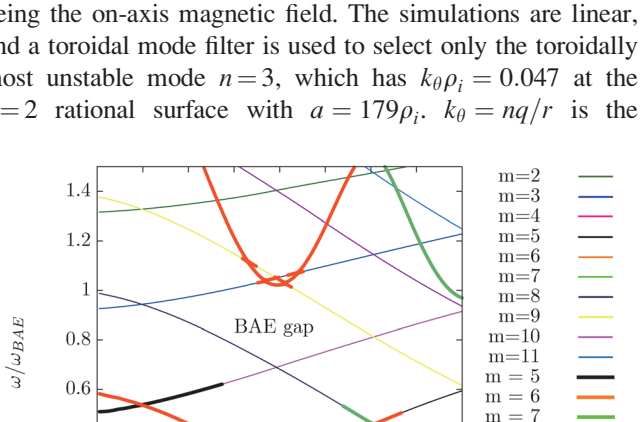

FIG. 1. Alfvén and sound continua solved for $n = 3$, $m \in [-20, 20]$ by an eigenvalue code ALCON. The thick lines are the Alfvén branches and the thin ones are the sound branches.

poloidal wave-vector and $\rho_i = \sqrt{m_i T_i}/eB_0$ is the thermal ion gyro-radius, where m_i is the ion mass. In this work, 64 grid points per poloidal wavelength, 40 particles per grid cell, and $0.01R_0/v_i$ per time step are used for a typical simulation. For the BAE, the parallel wave number is defined in terms of $k_\parallel = (nq - m)/qR \approx 0$, where R is the major radius at the rational surface. Considering the background plasma profile, according to Eq. (19), the accumulation point frequency is $\omega_{\mathrm{BAE}} = \sqrt{11T_i/2m_iR_0^2} \approx 2.34v_i/R_0$ with the ion thermal velocity $v_i = \sqrt{T_i/m_i}$ and it can correspond to the continuum spectrum (Fig. 1) of the $n = 3$ toroidal harmonic, which is obtained using an eigenvalue code called ALCON,[37] which solves the Alfvén continua with acoustic coupling. Meanwhile, only the $m = 5, 6, 7$ is kept by a poloidal filter to retain the sideband couplings.

For the BAE, the continuum spectrum around the same rational surface is almost the same for the different toroidal mode number. The dominant resonance is the precession frequency which is proportional to the toroidal mode number, which means that larger number of fast electrons satisfy the resonance condition for the high n mode, when the fast electrons have the Maxwell particle distribution. Meanwhile, the

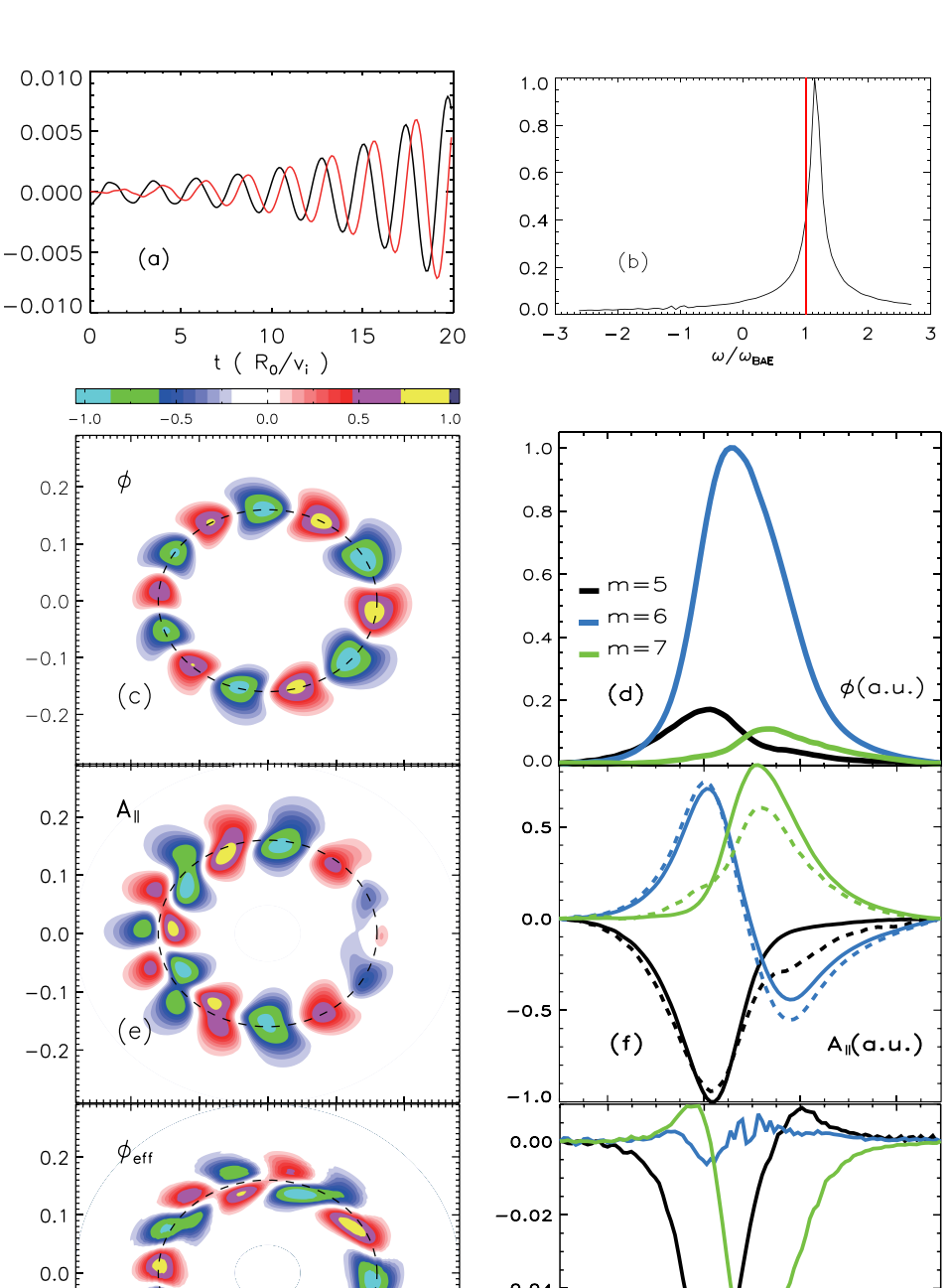

FIG. 2. The time history (a), frequency spectrum (b), poloidal mode structure (c), (e), and (g), and radial profiles (d), (f), and (h) of the electrostatic potential ϕ, the vector potential $A_\parallel$, and the effective potential ϕ_{eff}, for harmonics m = 5 (black), 6 (blue), and 7 (green). In panel (a), the black line is the real part and the red line is the imaginary part of the electrostatic potential. In panel (f), the solid line represents the actual $A_\parallel$ measured in simulation and the dotted line represents the $A_\parallel$ from the actual ϕ using the Faraday's law in the ideal MHD limit $\partial\delta A_\parallel/\partial t = -c\mathbf{b}_0 \cdot \nabla\phi$. In both panels (d) and (h), the normalization is the max ϕ of m = 6 harmonics.

fast electron's precessional drive should overcome the intrinsic damping of the background plasma, such as ion Landau damping,[38] continuum damping,[39,40] and radiative damping.[41] The damping mechanism determines only a range of toroidal mode number that is most unstable.[8] As a result, it is a balance that the $n=3$ mode is most unstable, which has been tested in the simulations, $n=2$ mode's growth rate is about 66.6% of the $n=3$ mode's growth rate, and $n=4$ mode's growth rate is about 95.7% of the $n=3$ mode's growth rate.

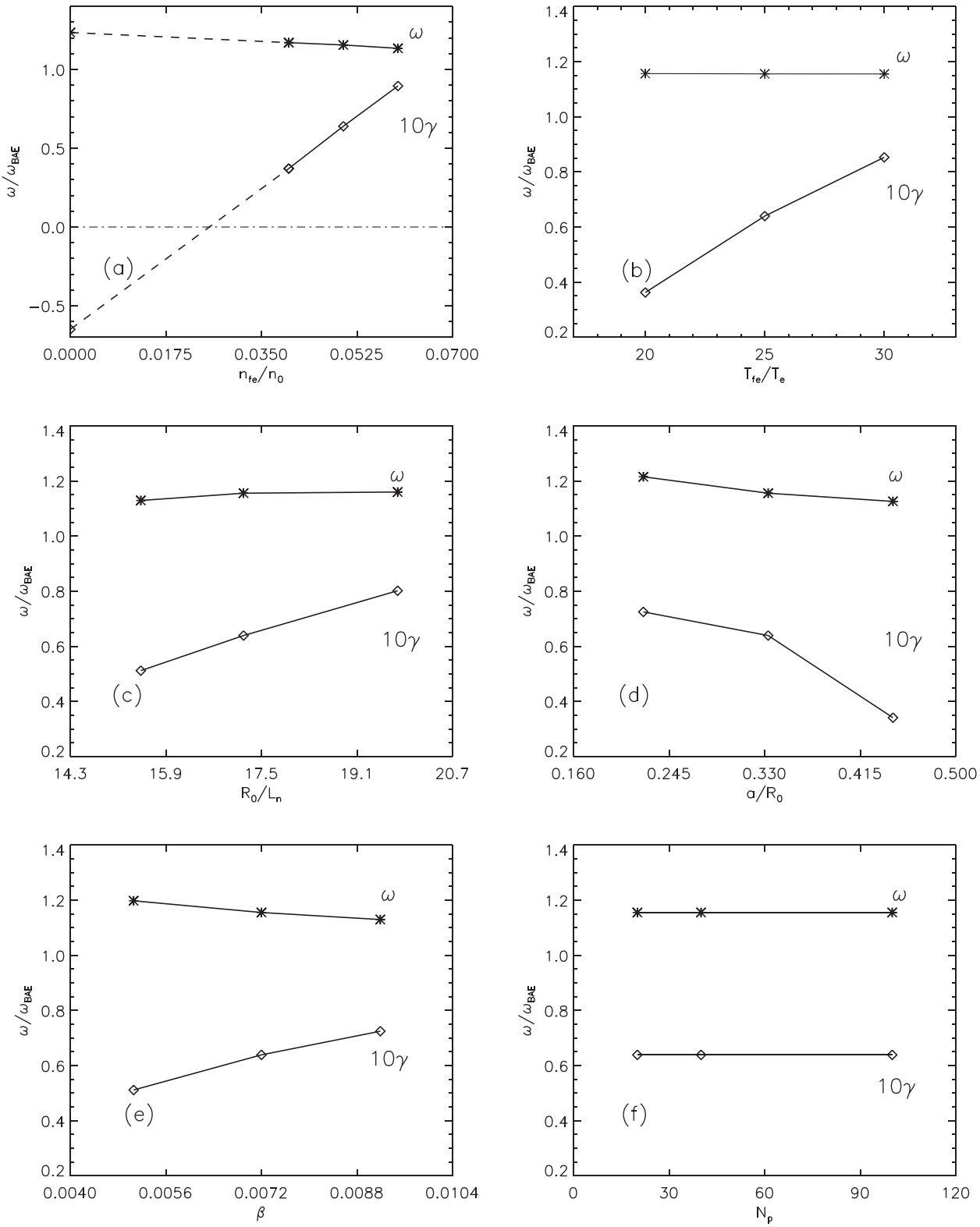

FIG. 3. Parameter scan of e-BAE frequency and linear growth rate: (a) fast electron density n_{fe} with constant $T_{fe}=25T_e$; (b) fast electron temperature T_{fe} with constant $n_{fe}=0.05n_e$; (c) fast electron density gradient R_0/L_n with constant $n_{fe}=0.05n_e$ and $T_{fe}=25T_e$; (d) aspect ratio a/R_0; (e) thermal plasma normalized pressure β; and (f) number of particle per cell N_p.

As shown in Figs. 2(a) and 2(b), e-BAE grows exponentially with a frequency of $\omega = 1.155\omega_{\mathrm{BAE}}$ and a linear growth rate of $\gamma = 0.0640\omega_{\mathrm{BAE}}$. The real part of the mode is $\pi/2$ leading the imaginary part in phase, which means that this wave is a traveling wave and propagates in the fast electron diamagnetic direction. Meanwhile, the poloidal mode structure of e-BAE in Fig. 2(c) shows an opposite direction (the triangular poloidal mode structure direction along the rational surface), compared with the fast-ion driven β-induced Aflvén (i-BAE) in Fig. 1(e) of Ref. 43. The reason is the different propagation direction of the i-BAE and e-BAE. The radial profiles for different harmonics in Fig. 2(d) shows that the sideband is about 1/5 of the dominant harmonics. The sideband can enhance the excitation of the e-BAE. When only $m = 6$ harmonics is kept in the simulation, the e-BAE will have a much lower growth rate. As show in Fig. 2(f), the $m = 6$ harmonics of $\delta A_{\parallel}$ is smaller compared with the sideband $m = 5$ and $m = 7$, since the $k_{\parallel}$ operator (i.e., $b_0 \cdot \nabla$) is relatively small ($k_{\parallel} \simeq 0$) for the m = 6 harmonics. Consistent with $A_{\parallel}$ profiles, the m = 6 harmonics is also much smaller in the effective potential ϕ_{eff}, compared with the adjacent sideband. Figs. 2(d) and 2(h) show that the effective potential is small, and Fig. 2(f) shows that the polarization of the excited BAE is close to an ideal MHD mode.

As an eigenmode, the e-BAE frequency changes slightly and locates around the accumulation point frequency when the fast electron density, temperature, or density gradient change (Figs. 3(a), 3(b), and 3(c)). Increasing n_{fe}, T_{fe}, or R_0/L_n will enhance the driven strength for e-BAE, leading to increase of the growth rate. The minimum square fitting of the points in Fig. 3(a) shows a nearly linear dependence on the mode real frequency and growth rate to the density ratio of fast electron to thermal electron. When the growth rate approaches zero, the fast electron density threshold can be estimated to be roughly 2% of thermal electron density. The background damping rate can be measured by the intercept point of the extrapolating line on the vertical axis, which is about $0.06\omega_{\mathrm{BAE}}$. In Fig. 3(d), the frequency and linear growth rate decrease with increasing the aspect ratio a/R_0, since the finite orbit width effect (FOW) is related to the aspect ratio, for example, the banana width of trapped ions is inversely proportional to the root of a/R_0. Meanwhile, in Fig. 3(e), when β increases, the frequency decreases but the linear growth rate increases, as BAE has strong interaction with the thermal plasmas.[9] As shown in Fig. 4(e), simulations with different number of particles per cell N_p shows that the number of particles is adequate in the simulation.

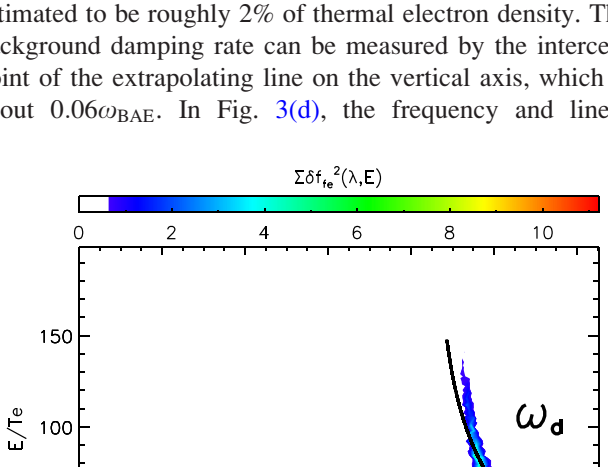

FIG. 4. Phase space (E, λ) structures of δf_{fe}^2. Solid line is resonance for trapped particles precessional frequency $\omega = \omega_d = n\omega_{pre}$ corresponding to e-BAE.

Generally speaking, the wave-particle resonance condition[64] of low-frequency waves is $\omega - k_{\parallel}v_{\parallel} - p\omega_t = 0$ for purely passing particles, and $\omega - n\omega_{pre} - p\omega_b = 0$ for deeply trapped particles, where p is an integer number, ω_t, ω_b, and ω_{pre}, are the guiding center transit, bounce, and precession frequencies, respectively. The relative strength of resonances can be inferred from the square of the perturbed distribution function of the fast electron[45,57] δf_{fe}^2 in the phase space. δf_{fe}^2 is a function of the equilibrium constants of motion (E, λ), where E is the guiding center kinetic energy and $\lambda = \mu B_0/E$ is a measurement of pitch angle. Fig. 4 shows that only the precessional resonance $(\omega = \omega_d \equiv n\omega_{pre})$ of the trapped fast electron is identified. The bounce averaged precession frequency ω_d for the trapped electron $(\kappa^2 = 2(r/R_0)\lambda/(1-(1-r/R_0)\lambda),\ 1 - r/R_0 < \lambda < 1 + r/R_0,\ \kappa^2 > 1)$[66–68] is obtained by the following equation:

$$\omega_d = \frac{nE}{eB_tR_0}\frac{q}{r}\left[\frac{2\mathbb{E}(1/\kappa)}{\mathbb{K}(1/\kappa)} - 1 + 4s\left(\frac{\mathbb{E}(1/\kappa)}{\mathbb{K}(1/\kappa)} + \frac{1}{\kappa^2} - 1\right) - \frac{\alpha}{2q^2} - \frac{4\alpha}{3}\left(1 - 1/\kappa^2 + \left(2/\kappa^2 - 1\right)\frac{\mathbb{E}(1/\kappa)}{\mathbb{K}(1/\kappa)}\right)\right], \tag{20}$$

where $s = rq'/q$ is the magnetic shear factor and $\alpha = -R_0q^2d\beta/dr$ is the pressure gradient in the (s, α) model tokamak equilibrium,[65] $\mathbb{K}$ and $\mathbb{E}$ stand for the complete elliptic integral of the first and second kind, respectively, and B_t is the toroidal field.

IV. SUMMARY

In this work, the fast-electron driven β-induced Alfvén eigenmodes (e-BAE) in toroidal plasmas is successfully verified in the gyrokinetic particle simulation by GTC. In our simulation, e-BAE is driven by the fast electron density gradient. The result shows that e-BAE propagates in the fast electron diamagnetic direction, and its polarization is close to an ideal MHD mode. The frequency of e-BAE changes slightly when the fast electron temperature, density, or density gradient changes. The growth rate increases slightly when the fast electron temperature, density, or density gradient increases. We find that the e-BAE frequency and linear growth rate are also sensitive to the thermal plasma's properties, such as aspect ratio a/R_0 and thermal plasma pressure β. The phase space structure shows that only the fast electron deeply trapped particle precession contributes to the resonance source.

In this work, the fast electrons are loaded as a local Maxwellian distribution for simplicity to demonstrate the code capability of e-BAE through linear verifications. Using the realistic equilibrium and profiles from experiment discharges, for example, the HL-2A experiments with ECRH heating, is our ongoing work and will be published in a future paper.

ACKNOWLEDGMENTS

Authors gratefully acknowledge useful discussions with F. Zonca, W. Chen, H. S. Zhang, and Chenxi Zhang.

This work was supported by the Chinese National Magnetic Confinement Fusion Science Program under Grant Nos. 2013GB111003 and 2013GB112011 and the National Natural Science Foundation of China under Grant No. 11275260. This research used resources of the National Supercomputer Center in Tianjin (NSCC-TJ), the Oak Ridge Leadership Computing Facility at Oak Ridge National Laboratory (DOE Contract No. DE-AC05-00OR22725), and the National Energy Research Scientific Computing Center (NERSC) (DOE Contract No. DE-AC02-05-CH11231).

[1]H. Alfvén, Nature **150**, 405 (1942).
[2]E. J. Strait, W. W. Heidbrink, A. D. Turnbull, M. S. Chu, and H. H. Duong, Nucl. Fusion **33**, 1849 (1993).
[3]M. Podestà, R. E. Bell, N. A. Crocker, E. D. Fredrickson, N. N. Gorelenkov, W. W. Heidbrink, S. Kubota, B. P. LeBlanc, and H. Yuh, Nucl. Fusion **51**, 063035 (2011).
[4]M. Garcia-Munoz, I. G. J. Classen, B. Geiger, W. W. Heidbrink, M. A. Van Zeeland, S. Äkäslompolo, R. Bilato, V. Bobkov, M. Brambilla, G. D. Conway, S. da Graça, V. Igochine, Ph. Lauber, N. Luhmann, M. Maraschek, F. Meo, H. Park, M. Schneller, G. Tradini, and ASDEX Upgrade Team, Nucl. Fusion **51**, 103013 (2011).
[5]M. S. Chu, J. M. Greene, L. L. Lao, A. D. Turnbull, and M. S. Chance, Phys. Fluids B **4**, 3713 (1992).
[6]F. Zonca, L. Chen, and R. A. Santoro, Plasma Phys. Controlled Fusion **38**, 2011 (1996).
[7]B. N. Breizman, M. S. Pekker, S. E. Sharapov, and JET-EFDA Contributors, Phys. Plasmas **12**, 112506 (2005).
[8]A. D. Turnbull, E. J. Strait, W. W. Heidbrink, M. S. Chu, H. H. Duong, J. M. Creene, L. L. Lao, T. S. Taylor, and S. J. Thompson, Phys. Fluids B **5**, 2546 (1993).
[9]F. Zonca, L. Chen, A. Botrubno, P. Buratti, A. Cardinali, R. Cesario, V. Pericoli Ridolfini, and JET-EFDA Contributors, Nucl. Fusion **49**, 085009 (2009).
[10]W. W. Heidbrink, E. J. Strait, M. S. Chu, and A. D. Turnbull, Phys. Rev. Lett. **71**, 855 (1993).
[11]R. Nazikian, Z. Chang, E. D. Fredrickson, E. Mazzucato, S. H. Batha, R. Bell, R. Budny, C. E. Bush, C. Z. Cheng, A. Janos, F. Levinton, J. Manickam, D. K. Mansfield, H. K. Park, G. Rewoldt, S. Sabbagh, E. J. Synakowski, W. Tang, G. Taylor, and L. E. Zakharov, Phys. Plasmas **3**, 593 (1996).
[12]W. W. Heidbrink, E. Ruskov, E. M. Carolipio, J. Fang, M. A. Van Zeeland, and R. A. James, Phys. Plasmas **6**, 1147 (1999).
[13]P. Buratti, P. Smeulders, F. Zonca, S. V. Annibaldi, M. De Benedetti, H. Kroegler, G. Regnoli, O. Tudisco, and FTU Team, Nucl. Fusion **45**, 1446 (2005).
[14]S. V. Annibaldi, F. Zonca, and P. Buratti, Plasma Phys. Controlled Fusion **49**, 475 (2007).
[15]O. Zimmermann, H. R. Koslowski, A. Kramer-Flecken, Y. Liang, R. Wolf, and TEC Team, in *Proceedings of 32nd EPS Conference on Plasma Physics, Tarragona, Spain*, 2005, p. 4.059.
[16]W. Chen, X. Q. Ji, Q. W. Yang, X. T. Ding, Y. Liu, B. B. Feng, Y. Huang, W. Li, Y. Zhou, J. Zhou, X. M. Song, L. C. Li, X. R. Duan, and HL-2A Team, J. Phys. Soc. Jpn. **79**, 044501 (2010).
[17]C. Nguyen, X. Garbet, R. Sabot, L.-G. Eriksson, M. Goniche, P. Maget, V. Basiuk, J. Decker, D. Elbeze, T. A. Huysmans, A. Macor, J.-L. Segui, and M. Schneider, Plasmas Phys. Controlled Fusion **51**, 095002 (2009).
[18]K. L. Wong, M. S. Chu, T. C. Luce, C. C. Petty, P. A. Politzer, R. Prater, L. Chen, R. W. Harvey, M. E. Austin, L. C. Johnson, R. J. La Haye, and R. T. Snider, Phys. Rev. Lett. **85**, 996 (2000).
[19]X. T. Ding, Y. Liu, G. C. Guo, E. Y. Wang, K. L. Wong, L. W. Yan, J. Q. Dong, J. Y. Cao, Y. Zhou, J. Rao, Y. Yuan, H. Xia, Y. Liu, and HL-1M Group, Nucl. Fusion **42**, 491 (2002).
[20]W. Chen, X. T. Ding, Q. W. Yang, Y. Liu, X. Q. Ji, Y. P. Zhang, J. Zhou, G. L. Yuan, H. J. Sun, W. Li, Y. Zhou, Y. Huang, J. Q. Dong, B. B. Feng, X. M. Song, Z. B. Shi, Z. T. Liu, X. Y. Song, L. C. Li, X. R. Duan, Y. Liu, and HL-2A Team, Phys. Rev. Lett. **105**, 185004 (2010).
[21]W. Chen, X. T. Ding, Y. Liu, Q. W. Yang, X. Q. Ji, G. L. Yuan, Y. P. Zhang, M. Isobe, Y. B. Dong, Y. Huang, J. Zhou, Y. Zhou, W. Li, B. B. Feng, X. M. Song, J. Q. Dong, Z. B. Shi, X. R. Duan, and HL-2A Team, Nucl. Fusion **51**, 063010 (2011).
[22]S. T. Tsai and L. Chen, Phys. Fluids B **5**, 3284 (1993).
[23]S. Briguglio, C. Kar, F. Romanelli, G. Vlad, and F. Zonca, Plasma Phys. Controlled Fusion **37**, A279 (1995).
[24]C. Z. Cheng, N. N. Gorelenkov, and C. T. Hsu, Nucl. Fusion **35**, 1639 (1995).
[25]R. Santoro and L. Chen, Phys. Plasmas **3**, 2349 (1996).
[26]N. N. Gorelenkov and W. W. Herdbrink, Nucl. Fusion **42**, 150 (2002).
[27]Z. Lin, T. S. Hahm, W. W. Lee, W. M. Tang, and R. B. White, Science **281**, 1835 (1998).
[28]I. Holod, W. L. Zhang, Y. Xiao, and Z. Lin, Phys. Plasmas **16**, 122307 (2009).
[29]Z. Lin, I. Holod, L. Chen, P. H. Diamond, T. S. Hahm, and S. Ethier, Phys. Rev. Lett. **99**, 265003 (2007).
[30]W. L. Zhang, Z. Lin, and L. Chen, Phys. Rev. Lett. **101**, 095001 (2008).
[31]Y. Xiao and Z. Lin, Phys. Rev. Lett. **103**, 085004 (2009).
[32]Y. Nishimura, Phys. Plasmas **16**, 030702 (2009).
[33]W. L. Zhang, I. Holod, Z. Lin, and Y. Xiao, Phys. Plasmas **19**, 022507 (2012).
[34]C. Z. Zhang, W. L. Zhang, Z. Lin, and D. Li, Phys. Plasmas **20**, 052501 (2013).
[35]Z. X. Wang, Z. Lin, I. Holod, W. W. Heidbrink, B. Tobias, M. Van Zeeland, and M. E. Austin, Phys. Rev. Lett. **111**, 145003 (2013).
[36]W. Deng, Z. Lin, and I. Holod, Nucl. Fusion **52**, 023005 (2012).
[37]W. Deng, Z. Lin, I. Holod, Z. Wang, Y. Xiao, and H. Zhang, Nucl. Fusion **52**, 043006 (2012).
[38]R. Betti and J. P. Freidberg, Phys. Fluids B **4**, 1465 (1992).
[39]M. N. Rosenbluth, H. L. Berk, J. W. Van Dam, and D. M. Lindberg, Phys. Rev. Lett. **68**, 596 (1992).
[40]F. Zonca and L. Chen, Phys. Rev. Lett. **68**, 592 (1992).
[41]R. R. Mett and S. M. Mahajan, Phys. Fluids B **4**, 2885 (1992).
[42]D. A. Spong, E. M. Bass, W. Deng, W. W. Heidbrink, Z. Lin, B. Tobias, M. A. Van Zeeland, M. E. Austin, C. W. Domier, and N. C. Luhmann, Jr., Phys. Plasmas **19**, 082511 (2012).
[43]H. S. Zhang, Z. Lin, I. Holod, X. Wang, Y. Xiao, and W. L. Zhang, Phys. Plasmas **17**, 112505 (2010).
[44]H. S. Zhang, Z. Lin, and I. Holod, Phys. Rev. Lett. **109**, 025001 (2012).
[45]H. S. Zhang, Z. Lin, W. Deng, I. Holod, Z. X. Wang, Y. Xiao, and W. L. Zhang, Phys. Plasmas **20**, 012510 (2013).
[46]J. McClenaghan, Z. Lin, I. Holod, W. Deng, and Z. Wang, Phys. Plasmas **21**, 122519 (2014).
[47]D. J. Liu, W. L. Zhang, J. McClenaghan, J. Q. Wang, and Z. Lin, Phys. Plasmas **21**, 122520 (2014).
[48]A. Kuley, Z. Lin, J. Bao, X. S. Wei, Y. Xiao, W. Zhang, G. Y. Sun, and N. J. Fisch, Phys. Plasmas **22**, 102515 (2015).
[49]J. Bao, Z. Lin, A. Kuley, and Z. X. Lu, Plasmas Phys. Controlled Fusion **56**, 095020 (2014).
[50]S. Briguglio, F. Zonca, and G. Vlad, Phys. Plasmas **5**, 3287 (1998).
[51]X. Wang, S. Briguglio, L. Chen, D. Di Troia, G. Fogaccia, G. Vlad, and F. Zonca, Phys. Plasmas **18**, 052504 (2011).
[52]X. Wang, F. Zonca, and L. Chen, Plasma Phys. Controlled Fusion **52**, 115005 (2010).
[53]X. Wang, S. Briguglio, L. Chen, C. Di Troia, G. Fogaccia, G. Vlad, and F. Zonca, Phys. Rev. E **86**, 045401(R) (2012).
[54]W. Park, E. V. Belova, G. Y. Fu, X. Z. Tang, H. R. Strauss, and L. E. Sugiyama, Phys. Plasmas **6**, 1796 (1999).
[55]W. Park, J. Breslau, J. Chen, G. Y. Fu, S. C. Jardin, S. Klasky, J. Menard, A. Pletzer, B. C. Stratton, D. Stutman, H. R. Strauss, and L. E. Sugiyama, Nucl. Fusion **43**, 483 (2003).
[56]A. J. Brizard and T. S. Hahm, Rev. Mod. Phys. **79**, 421 (2007).
[57]H. S. Zhang and Z. Lin, Phys. Plasmas **17**, 072502 (2010).

[58]Y. Nishimura, Z. Lin, and W. X. Wang, Phys. Plasmas **14**, 042503 (2007).
[59]Z. Lin and L. Chen, Phys. Plasmas **8**, 1447 (2001).
[60]Z. Lin, Y. Nishimura, Y. Xiao, I. Holod, W. L. Zhang, and L. Chen, Plasma Phys. Controlled Fusion **49**, B163 (2007).
[61]W. W. Lee, J. Comput. Phys. **72**, 243 (1987).
[62]Z. Lin and W. W. Lee, Phys. Rev. E **52**, 5646 (1995).
[63]H. Biglari and L. Chen, Phys. Rev. Lett. **67**, 3681 (1991).
[64]L. Chen, J. Geophys. Res. **104**, 2421, doi:10.1029/1998JA900051 (1999).
[65]J. W. Connor, R. J. Hastie, and J. B. Taylor, Phys. Rev. Lett. **40**, 396 (1978).
[66]J. P. Graves, R. J. Hastie, and K. I. Hopcraft, Plasma Phys. Controlled Fusion **42**, 1049 (2000).
[67]M. Rosenbluth and M. L. Sloan, Phys. Fluids **14**, 1725 (1971).
[68]J. W. Connor, R. J. Hastie, and T. J. Martin, Nucl. Fusion **23**, 1702 (1983).